

Ptychographic reconstruction of pure quantum states

M. F. Fernandes^{*} and L. Neves[†]

Departamento de Física, Universidade Federal de Minas Gerais, Belo Horizonte, MG 31270-901, Brazil

(Dated: December 15, 2024)

Ptychography is an imaging technique in which a localized illumination scans overlapping regions of an object and generates a set of diffraction intensities used to computationally reconstruct its transmission function. We propose a quantum analogue of this technique designed to reconstruct d -dimensional pure states. A set of n rank- r projectors “scans” overlapping parts of an input state and the moduli of the d Fourier amplitudes of each part are measured. These nd outcomes are fed into an iterative phase retrieval algorithm which estimates the state. For d up to 100 and $r = \lfloor d/2 \rfloor$, we performed numerical simulations for single systems in an economic ($n = 4$) and a costly ($n = d$) scenario, as well as for multiqubit systems ($n = 6 \log d$), all yielding, in general, reconstructions with infidelities below 10^{-5} . The method is shown to be resilient to noise and, for any d , requires a simple and fast postprocessing algorithm. Unlike traditional approaches to state reconstruction, the ptychographic scheme uses a single measurement basis; the diversity and redundancy in the measured data—key for its success—are provided by the overlapping projections. We illustrate the simplicity of this scheme with the paradigmatic multiport interferometer.

The quantum state of a physical system fully characterizes it and its knowledge allows one, for instance, to predict any possible measurement outcome, estimate relevant quantities for quantum information processing, and determine quantum dynamics. Therefore, the ability to reconstruct quantum states is fundamental both from the operational point of view and for the development of quantum technologies [1]. In a standard approach, this task is carried out by making projective measurements (from suitably chosen bases) on identically prepared quantum systems, estimating the outcome probabilities, and feeding them into some postprocessing algorithm that will deliver a physical state compatible with the data set [2, 3]. This process, known as quantum state tomography, has become an integral part of the quantum information toolbox [3–8].

The complexity of quantum tomography increases with the state-space dimension, d , as the required number of measurement bases (or unitary operations on the system) scales, at least, with d [9–11]. However, under prior information the process is simplified. For example, if an unknown state is known to be pure, four [12–14] or five [13, 15] measurement bases and simple postprocessing suffice for determining it on any dimension. Yet, to implement the measurements in a variety of bases (or, equivalently, to implement various unitary operations) may not be straightforward in all experiments.

In this work, we introduce a method for pure state reconstruction that, unlike a typical tomography, uses a single basis in which partially overlapping parts of the unknown state are measured. Additionally, it employs a simple and fast iterative phase retrieval algorithm for postprocessing. The method is based on *ptychography* [16–18], a powerful coherent diffractive imaging (CDI) technique applied, specially, in optical [19–21]

and electron [22, 23] microscopy. A typical setup for ptychography is sketched in Fig. 1(a): a plane wave filtered by a pinhole creates a localized illumination probe on the object to be imaged; in the far field, one measures the intensity of the generated diffraction pattern (Fourier intensity). The ptychographic CDI process is carried out by scanning the probe over partially overlapping parts of the object and recording the corresponding Fourier intensities. When both the illumination probe and its positioning are accurately known *a priori*, this data set and the probe information are fed into an iterative algorithm, called ptychographic iterative engine (PIE) [24, 25]. Starting with a random or uniform estimate for the complex-valued object transmission function, the PIE will iteratively update it by applying the overlap and moduli constraints [26], and will stop when some terminating condition is met. The implicit phase corrections, resulting from moduli imposition in the conjugate domain, together with the diversity and redundancy in the data, enforced by the multiple overlapping illuminations, make the initial estimate converge to the object function. Figure 1(b) outlines the process.

In the proposed quantum analogue of ptychographic CDI, sketched in Fig. 1(c), a set of n projectors “scans” overlapping parts of an input pure state and the moduli of the d Fourier amplitudes of each part are measured. These nd outcomes are fed into a PIE-based algorithm which estimates the state. For d up to 100, we simulated numerically the ptychographic reconstruction for states of single systems using $n = 4$ and $n = d$, and multiqubit systems using $n = 6 \log d$ projectors. Considering both noise-free and noisy scenarios, we obtained successful reconstructions in all cases. Finally, through the paradigmatic multiport interferometer [27], we illustrate the simplicity of our method in comparison with typical tomographic approaches.

An arbitrary pure quantum state in a d -dimensional Hilbert space \mathcal{H}_d may be written in the computational basis $\{|k\rangle\}_{k=0}^{d-1}$ as $|\psi\rangle = \sum_{k=0}^{d-1} c_k |k\rangle$, where $\sum_k |c_k|^2 = 1$.

^{*} fernandes-mario@ufmg.br

[†] lneves@fisica.ufmg.br

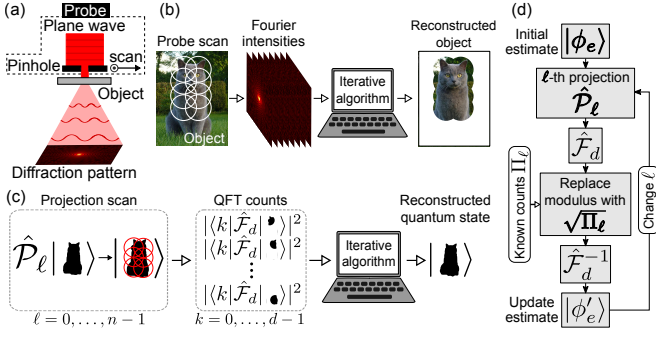


FIG. 1. (a) Schematic of a typical ptychography setup. (b) Ptychographic imaging process. (c) Quantum state ptychography. (d) PIE diagram. See text for details.

This is the object we want to reconstruct by determining the d complex coefficients $\{c_k\}_{k=0}^{d-1}$, which completely specify it. In our ptychographic approach, the role of the localized, scanning, and partially overlapping illumination probe will be played by a set of n projectors $\{\hat{\mathcal{P}}_\ell\}_{\ell=0}^{n-1}$ onto r -dimensional subspaces ($1 < r < d$) of \mathcal{H}_d . For this set of rank- r probe projectors we impose two conditions: (i) each projector in the set must have a partial overlap with at least one other partner, i.e., for any $\hat{\mathcal{P}}_\ell$ there exists a $\hat{\mathcal{P}}_{\ell'}$ such that $0 < \mathcal{O} \equiv \text{Tr}(\hat{\mathcal{P}}_\ell \hat{\mathcal{P}}_{\ell'})/r < 1$; (ii) all levels in \mathcal{H}_d must be addressed at least once. The most straightforward set satisfying the above requirements is formed by projectors which are diagonal in the computational basis. In particular, we consider, initially, projectors given by

$$\hat{\mathcal{P}}_\ell = \sum_{j=0}^{r-1} |j \oplus s_\ell\rangle \langle j \oplus s_\ell|, \quad (1)$$

where \oplus denotes addition modulo d and s_ℓ is a nonnegative integer that sets the skip between adjacent operators and may be arranged in a n -entry vector $\mathbf{s}^{(n)} = (s_0, \dots, s_{n-1})$. The parameters n , r , and $\mathbf{s}^{(n)}$ which characterize the set of probe projectors will be specified later.

Given an ensemble of d -dimensional quantum systems described by the state $|\psi\rangle$, the ptychographic measurements on this state proceeds as follows: we first apply the ℓ -th probe projection on the input ensemble, generating an output sub-ensemble described by the (unnormalized) state $|\psi_\ell\rangle = \hat{\mathcal{P}}_\ell |\psi\rangle$. Next, we apply a quantum Fourier transform (QFT) on this output, obtaining: $|\tilde{\psi}_\ell\rangle = \hat{\mathcal{F}}_d |\psi_\ell\rangle = \sum_{k=0}^{d-1} \tilde{c}_{k\ell} |k\rangle$, where $\hat{\mathcal{F}}_d$ is the QFT acting on \mathcal{H}_d and $\{\tilde{c}_{k\ell}\}_{k=0}^{d-1}$ is the set of Fourier transformed amplitudes of $|\psi_\ell\rangle$. Finally, we perform a projective measurement in the computational basis. This procedure is repeated for each $\hat{\mathcal{P}}_\ell$ and gives us a set of n count distributions $\{\Pi_\ell = \{\mathcal{N}|\tilde{c}_{k\ell}|^2\}_{k=0}^{d-1}\}_{\ell=0}^{n-1}$, where \mathcal{N} is a constant dependent on the particle flux and detector efficiencies [28]. These distributions form our ptychographic data set as $\{\sqrt{\Pi_\ell}\}_{\ell=0}^{n-1}$, which, together with the *a priori* known set of probe projectors, will be the inputs to an iterative phase retrieval algorithm designed to reconstruct

$|\psi\rangle$. The entire process of quantum state ptychography is illustrated in Fig. 1(c).

Our iterative reconstruction algorithm is an adapted version of the PIE [24, 25] and works in the following manner. (1) Start with a random estimate of the input state in the computational basis: $|\phi_e\rangle = \sum_{k=0}^{d-1} \gamma_k |k\rangle$. (2) Apply the ℓ -th probe projector to $|\phi_e\rangle$: $|\phi_{e,\ell}\rangle = \hat{\mathcal{P}}_\ell |\phi_e\rangle$. (3) Apply the QFT to the output estimated state: $|\tilde{\phi}_{e,\ell}\rangle = \hat{\mathcal{F}}_d |\phi_{e,\ell}\rangle = \sum_{k=0}^{d-1} \tilde{\gamma}_{k\ell} |k\rangle$. (4) Use the ℓ -th measured ptychographic data, $\sqrt{\Pi_\ell}$, to correct the moduli of the coefficients of $|\tilde{\phi}_{e,\ell}\rangle$, keeping their phases: $|\tilde{\phi}_{c,\ell}\rangle = \sqrt{\mathcal{N}} \sum_{k=0}^{d-1} |\tilde{c}_{k\ell}| e^{i \arg \tilde{\gamma}_{k\ell}} |k\rangle$. (5) Apply the inverse QFT to obtain an updated estimate for the output state: $|\phi_{c,\ell}\rangle = \hat{\mathcal{F}}_d^{-1} |\tilde{\phi}_{c,\ell}\rangle$. (6) Update the current estimate of the input state: $|\phi'_e\rangle = |\phi_e\rangle + \beta \hat{\mathcal{P}}_\ell (|\phi_{c,\ell}\rangle - |\phi_{e,\ell}\rangle)$, where β is a feedback parameter, roughly within $(0, 2]$, that controls the step-size of the update and can be adjusted to improve convergence (see Appendix). (7) Use this updated estimate as input to repeat the steps (2)–(6) with a new value of ℓ . This sequence is summarized in the diagram of Fig. 1(d): a single PIE iteration consists of n iterations through the closed loop [steps (2)–(7)], where each probe projector and corresponding ptychographic data is used once to update the state estimate. At each iteration we calculate the relative distance between the current and updated estimates, i.e., $D = \|\phi'_e - \phi_e\|^2 / \|\phi_e\|^2$; the algorithm terminates when it achieves either a sufficiently small value of D or a preset maximum number of PIE iterations, delivering a pure state that must be normalized.

The ptychographic method requires a total of $\mathcal{M} = nd$ measurement outcomes— d QFT state-amplitudes for each of the n probe projections. In this regard, its experimental cost will be determined by the number of $\hat{\mathcal{P}}_\ell$'s adopted. Along with the parameters r and $\mathbf{s}^{(n)}$, this number also defines the diversity of the data set and its degree of redundancy arising from the partially overlapping projections. Here, we set $n = 2, \dots, d$: the minimum follows directly from the requirements for these projectors, whereas the maximum was our choice to obtain a high diversity for the measured data and keep $\mathcal{M}_{\max} = d^2$, that is the usual \mathcal{M} in a standard implementation of quantum state tomography. As we will see next, a high value of n , although experimentally more demanding, provides more diversity and redundancy in the data, improving the PIE's convergence and the quality of the reconstruction. For a low value of n , the scenario is the opposite.

The performance of the protocol has been analyzed in numerical simulations for $n = 4$ and $n = d$ probe projectors, which gives $\mathcal{M} = 4d$ and $\mathcal{M} = d^2$, respectively. The first case compares with the recently demonstrated result that four observables in \mathcal{H}_d (thus $\mathcal{M} = 4d$) suffice to reconstruct all pure states up to a set of measure zero of dimension $d - 2$ [13]. The second case uses what would be an overcomplete data set to reconstruct pure states. Once n is settled, what remains is to define the rank r and the skip vector $\mathbf{s}^{(n)}$

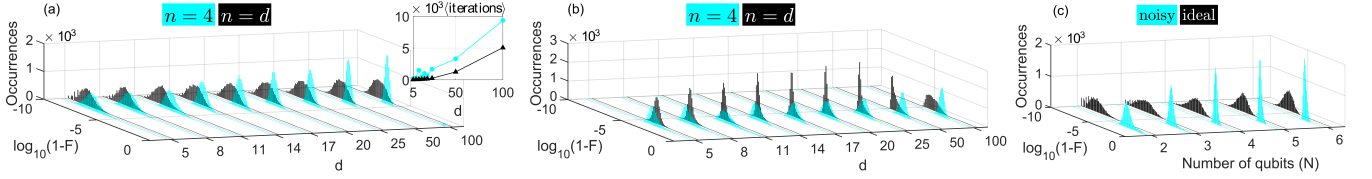


FIG. 2. Histograms of infidelity for ptychographically reconstructed quantum states (10^4 random states per histogram). [(a) and (b)] Simulations for d -dimensional states using $n = 4$ and $n = d$ probe projectors, performed with (a) ideal and (b) noisy data; the inset in (a) shows the average number of iterations until convergence of the PIE for each measurement scheme. Results for $d = 3$ and 4 were omitted for clarity. (c) Simulations for N -qubit states using ideal and noisy data.

which completely specify the $\hat{\mathcal{P}}_\ell$'s [Eq. (1)] and their overlap \mathcal{O} . Despite some freedom, one can choose these parameters based on how they improve the performance of the reconstruction algorithm. For $n = d$, we set $\mathbf{s}^{(d)} = (0, 1, \dots, d-1)$ and found that a rank around $\lfloor d/2 \rfloor$ optimizes the PIE's convergence (see Appendix). Here, we used $r = \lfloor d/2 \rfloor$ (except for $d = 3$, where $r = 2$) which gives $\mathcal{O} = 1 - 1/r$. This rank has also been adopted for $n = 4$, while $\mathbf{s}^{(4)} = (0, \lceil \frac{d-r-2}{3} \rceil, 2\lceil \frac{d-r-2}{3} \rceil, \lceil \frac{d}{2} \rceil)$ was chosen to give a good average overlap ($\approx d/3 \lceil d/2 \rceil$).

Using the two sets of probe projectors described above, our study comprised several dimensions from $d = 3$ to $d = 100$. For each d , 10^4 input quantum states were randomly generated according to the Haar measure. The ptychographic data sets produced from these states were fed into the PIE algorithm, which was ran with a feedback parameter $\beta = 1.5$, optimized numerically as shown in the Appendix. Our stop criteria consisted of two clauses: reaching $D < 10^{-8}$ ($D < 10^{-5}$) for tests with ideal (noisy) data or 100 PIE iterations, whichever happened first. If the algorithm was stopped by the second clause, we allowed for a reinitialization and a new run, and used up to 100 reinitializations. At the end, the quality of the reconstruction is quantified by computing the fidelity $F = |\langle \phi_{\text{PIE}} | \psi \rangle|^2$ and infidelity $I = 1 - F$ between the input state, $|\psi\rangle$, and the normalized estimate of the algorithm, $|\phi_{\text{PIE}}\rangle$.

In the first test, we assumed a noise-free scenario. The resulting infidelities are shown in the histograms of Fig. 2(a). It can be seen that they are significantly lower for the scheme with $n = d$ (black data) than with $n = 4$ (cyan data) probe projectors. The computed median of the histograms increased with d in the range of 5.9×10^{-9} to 1.1×10^{-7} in the first case and 9.3×10^{-8} to 3.2×10^{-6} in the second case, giving an order of magnitude difference between them. Nevertheless, the overall performance of the protocol was excellent in both cases, with $I < 10^{-5}$ for the vast majority of reconstructions when $n = 4$ and for all reconstructions when $n = d$. The inset of Fig. 2(a) shows the average number iterations until convergence of the PIE as a function of d for each measurement scheme [29]. All these results confirm that the scheme with more probe projections outperforms the one with less, regarding both the quality of the reconstructions and the speed of PIE's convergence. Even so, the more economic procedure still gave very good results. In this case, the algo-

rithm will have to handle ptychographic data sets with less redundancy and diversity (which can be related to the ratio n/d). Thus, it will find more difficulty to reconstruct the states, especially for high dimensions. In $d = 100$, for instance, about 4% of input states have not been well characterized. A straightforward way to overcome this issue is including one or a few more probe projector(s) in the measurement at the expense of increasing the experimental cost. Alternatively, one may implement the recent improvements in the PIE that successfully handle difficult data sets [30], but this is beyond the scope of this work.

Despite the rapid growth in the number of iterations with state-space dimension seen in the inset of Fig. 2(a), the processing times of the PIE algorithm were very short. For $d = 100$ and $n = 4$, the reconstructions lasted around one second per state on a modest laptop. The other results were obtained in fractions of this time, showing that the postprocessing in our method is not only simple, but also fast, which is particularly important for high dimensions.

In the second test, we examined the resilience of the ptychographic protocol against noise. The imperfect generation of states and the random nature of detections were simulated with depolarization and Poissonian noise, respectively. The first can be modeled as a random fluctuation in the density matrix of the pure state ($|\psi\rangle\langle\psi|$), so that the generated state will be $\hat{\rho} = (1-\eta)|\psi\rangle\langle\psi| + \eta\hat{\rho}_{\text{rand}}$, where η is the noise level, and the random perturbation $\hat{\rho}_{\text{rand}}$ is drawn according to the Haar measure in the mixed states space. The diagonal components of $\hat{\mathcal{F}}_d \hat{\mathcal{P}}_\ell \hat{\rho} \hat{\mathcal{P}}_\ell \hat{\mathcal{F}}_d^{-1}$, denoted by $\{|\tilde{C}_{k\ell}|^2\}_{k=0}^{d-1}$, provided the simulated data to which we applied a Poisson distribution of average $\lambda|\tilde{C}_{k\ell}|^2$, where λ is a count rate factor. In our simulations we used realistic values of $\eta = 0.05$ and $\lambda = 10^3$ [5, 11] (see also the Appendix). Note that the PIE algorithm will treat the noisy data as if they came from a pure state, and it will deliver a pure state as well. Figure 2(b) shows the histograms of infidelity obtained in this case; overall, $I < 10^{-2}$. We can draw similar conclusions here as in the ideal case in the comparison between the schemes with $n = d$ and $n = 4$ projectors, but only now with the infidelities getting worse. Yet, the good quality of the reconstructions under noisy conditions is evident from these results and shows the robustness of the ptychographic method in a realistic scenario.

To highlight the role of the overlap between probe projectors in the ptychographic measurements, we also simulated reconstructions using nonoverlapping $\hat{\mathcal{P}}_\ell$'s. For $d = 20$, $n = 4$, $r = 5$, $\mathbf{s}^{(4)} = (0, 5, 10, 15)$ in Eq. (1), and 10^4 random states, we obtained fidelities ranging from 10^{-4} to 0.81 with an average of 0.15. These results show that the multiple overlaps are crucial in the protocol: without them, the ptychographic problem becomes several disjoint standard phase retrieval problems [31], which are known to suffer from nonuniqueness and stagnation issues [32].

Let us now discuss how our method deals with the reconstruction of sparse pure states, i.e., states in which most of the components are zero. In this case, it will succeed only if every nonzero component is addressed with at least one other nonzero component by some probe projector, so that they can interfere. Otherwise, we will fall into a disjoint group of phase retrieval problems as discussed above. One way to ensure this is to use the already considered set of $n = d$ probe projectors [Eq. (1) with $\mathbf{s}^{(d)} = (0, 1, \dots, d-1)$], but now with rank $r \geq \lfloor d/2 \rfloor + 1$, because when the levels of \mathcal{H}_d are addressed cyclically, the biggest distance between nonzero components will be $\lfloor d/2 \rfloor$. A second way is to use an adaptive approach: first, one measures in the computational basis; if the state is verified to be sparse, then one applies the ptychographic method building the probe projectors according to the distribution of its nonzero components.

For the ptychography in an N -qubit system, most of the projectors defined in Eq. (1) would not be factorable in the chosen initial basis. To work in a simpler scenario, we considered a fixed set of $n = 6N$ local probe projectors given by $\hat{\mathcal{P}}_{\ell j} = \hat{\pi}_{\ell j} \otimes \hat{\mathbb{I}}_2^{\otimes N-1}$, where $\hat{\pi}_{\ell j} = |\ell_j\rangle\langle\ell_j|$ are projectors onto the eigenstates of the Pauli operators $\hat{\sigma}_x$ ($\ell = +, -$), $\hat{\sigma}_y$ ($\ell = R, L$) and $\hat{\sigma}_z$ ($\ell = 0, 1$), and $\hat{\mathbb{I}}_2$ is the identity in the qubit space. The ℓ -th $\hat{\pi}_{\ell j}$ acts on the j -th qubit ($j = 1, \dots, N$) whereas the remaining qubits are left unchanged. These probe projectors have rank $r = 2^{N-1}$ and an overlap $\mathcal{O} = 1/2 + \delta_{jj'}(|\langle\ell|\ell'\rangle|^2 - 1/2)$; some of them do not address contiguous levels of \mathcal{H}_d and those with $\ell \neq 0, 1$ are not diagonal in the computational basis. The protocol follows the same steps described earlier. For $N = 2$ to 6 qubits, we have simulated the ptychographic reconstruction of 10^4 random pure states in noise-free and noisy scenarios, both yielding excellent results as shown in the histograms of infidelity of Fig. 2(c). The PIE's convergence took, on average, 200 iterations for $N = 6$. We attribute this fast convergence to the structure of the probe projectors $\hat{\mathcal{P}}_{\ell j}$, which allows the algorithm to access the levels of \mathcal{H}_d in a more distributed manner.

To illustrate the simplicity of the quantum ptychographic scheme and discuss other of its general aspects, let us consider d -dimensional states encoded in the propagation modes of single photons. A multiport interferometer (MI), sketched in Fig. 3 (right) for $d = 8$, can implement any unitary transformation on this encoding [27]. Under these circumstances, the probe projectors given by Eq. (1) would be realized by mode filters at

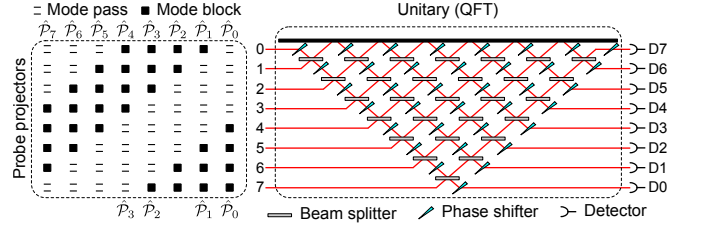


FIG. 3. Scheme for ptychographic reconstruction of 8-dimensional quantum states in a multiport interferometer using $n = 8$ (top) or $n = 4$ (bottom) rank-4 probe projectors.

the input ports of the interferometer, as shown in Fig. 3 (left). By setting the MI to perform $\hat{\mathcal{F}}_d$, the ptychographic data would be collected simply by shifting the mode filters n times at the input ports and recording the counts at the output ports. For comparison, to reconstruct these states by measuring four or five observables [12–15], the mode filters would not be necessary, but one would have to reconfigure the whole MI for each measurement basis employed. This shows a nice feature of the ptychographic method: the measurements are effectively performed in a single basis while the probe projectors are “shifted” through the Hilbert space.

We have proposed and numerically studied a method to reconstruct pure quantum states based on ptychography [16–18]. Successful reconstructions obtained in ideal and noisy scenarios make our ptychographic approach amenable to future experiments and a concrete alternative to standard tomographic techniques [12–15]. Since the emergence of ptychography in its modern form [18, 24], the technique has evolved impressively. Subsequent advances included, in special, the recovery of the illumination probe [33], the use other propagators rather than the Fourier transform [34], and the handling of mixedness both in the probe and in the object [35]. Our method, based on the simplest form of ptychography [18], may follow a similar route and be extended in many directions, including the utilization of different types of probe operators and different measurement bases, the reconstruction of mixed states and processes both in discrete and continuous domains, among others.

Acknowledgements: This work was supported by FAPEMIG (APQ-00240-15) and INCT-Informação Quântica. M. F. F. acknowledges financial support from CNPq.

APPENDIX

a. Optimization of the feedback parameter

In our adapted version of the PIE algorithm described in the main text, the sixth step consists of updating the current state estimate ($|\phi_e\rangle$) according to $|\phi'_e\rangle =$

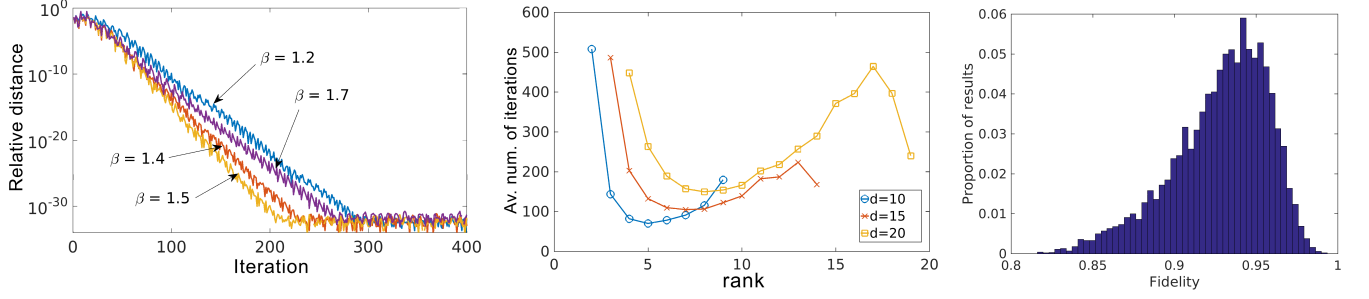


FIG. 4. (Left panel) Evolution of the relative distance in the state estimate for different values of the feedback parameter, β . We found $\beta = 1.5$ to achieve the fastest decrease, meaning that the PIE algorithm converged at a higher rate. (Center panel) Average number of iterations until convergence of the PIE algorithm as a function of the probe projector rank. Ranks around $\lfloor d/2 \rfloor$ made the algorithm converge faster. (Right panel) Histogram of degraded fidelities.

$|\phi_e\rangle + \beta \hat{\mathcal{P}}_\ell(|\phi_{c,\ell}\rangle - |\phi_e\rangle)$, where β is a feedback parameter for the algorithm and is roughly within $(0, 2]$. It controls the step-size of the update and can be adjusted to improve convergence: for $\beta = 1$, the algorithm corrects the estimate strictly in the subspace spanned by $\hat{\mathcal{P}}_\ell$; higher values can make it progress faster and converge in less iterations; lower values can make it slower but more stable. Using the same initial estimated and target state, we obtained the optimal β by running the PIE and recording the relative distance, $D = \|\phi'_e - \phi_e\|^2 / \|\phi_e\|^2$, in the estimation at each iteration, for several values of the parameter. Figure 4 shows the evolutions for a few values of β we tested. The best progression was achieved by $\beta = 1.5$, which we used in all later studies.

b. Optimal rank of the probe projectors

Let the set of n rank- r probe projectors defined in Eq. (1) of the main text be specified by $n = d$ and $\mathbf{s}^{(d)} = (0, 1, \dots, d-1)$. To determine the optimal r for the ptychographic measurements in this case, we studied the convergence of the PIE algorithm as a function of this rank for a few state-space dimensions ($d = 5, 10, 15$). For each combination of d and r , we reconstructed 10^4 random states and calculated the average number of iterations necessary until convergence. The results are shown in Fig. 4 and indicate that a rank around $\lfloor d/2 \rfloor$ works best. In our simulations we have chosen to use $r = \lfloor d/2 \rfloor$, but any other closer value would provide similar results regarding the quality of the reconstruction.

c. Noise levels in the simulation

We introduced depolarization and Poissonian noise in the ptychographic data to study if the protocol would still work in a realistic scenario. As mentioned in the main text, we based our noise levels on experiments found in the literature, but we still wanted to verify if they were indeed realistic. To this end, we picked 10^4 random pure states, degraded their amplitudes with the two modalities of noise and computed the fidelities with the original states. That is, after picking a random state $|\psi\rangle = \sum_j \mu_j |j\rangle$, we introduced depolarization noise, resulting in

$$\hat{\rho}_{\text{dep}} = (1 - \eta)|\psi\rangle\langle\psi| + \eta\hat{\rho}_{\text{rand}}, \quad (2)$$

where $\hat{\rho}_{\text{rand}}$ is a random mixed state and η is the noise level (we used $\eta = 0.05$). We then calculated the amplitudes of this state in the computational basis,

$$\mu_{k \text{ dep}} = \sqrt{\langle k | \hat{\rho}_{\text{dep}} | k \rangle}, \quad (3)$$

and applied Poissonian noise to the respective intensities,

$$\mu'_k{}^2 = \text{Poisrnd}(\lambda(\mu_{k \text{ dep}})^2), \quad (4)$$

where λ denotes the average count rate and $\text{Poisrnd}(x)$ denotes a random pick of the Poisson distribution with average x . Using $\lambda = 10^3$, we finally construct the amplitude-degraded state

$$|\psi'\rangle = \sum_j \frac{\mu'_j e^{i \arg \mu_j}}{\sqrt{\sum_k \mu'_k{}^2}} |j\rangle \quad (5)$$

and compute its fidelity with $|\psi\rangle$, namely $|\langle\psi'|\psi\rangle|^2$. Figure 4 shows a histogram of the degraded fidelities, which are indeed comparable—and even lower—to what is found in the literature [36].

-
- [1] M. A. Nielsen and I. L. Chuang, *Quantum Computation and Quantum Information* (Cambridge University Press, Cambridge, 2000).
- [2] W. K. Wootters and B. D. Fields, *Ann. Phys.* **191**, 363 (1989).
- [3] D. F. V. James, P. G. Kwiat, W. J. Munro, and A. G. White, *Phys. Rev. A* **64**, 052312 (2001).
- [4] R. T. Thew, K. Nemoto, A. G. White, and W. J. Munro, *Phys. Rev. A* **66**, 012303 (2002).
- [5] D. Gross, Y.-K. Liu, S. T. Flammia, S. Becker, and J. Eisert, *Phys. Rev. Lett.* **105**, 150401 (2010).
- [6] R. B. A. Adamson and A. M. Steinberg, *Phys. Rev. Lett.* **105**, 030406 (2010).
- [7] T. O. Maciel, A. T. Cesário, and R. O. Vianna, *Int. J. Mod. Phys. C* **22**, 1 (2011).
- [8] G. Lima, L. Neves, R. Guzmán, E. S. Gómez, W. A. T. Nogueira, A. Delgado, A. Vargas, and C. Saavedra, *Opt. Express* **19**, 3542 (2011).
- [9] H. Häffner, W. Hänsel, C. F. Roos, J. Benhelm, D. C. al kar, M. Chwalla, T. Körber, U. D. Rapol, M. Riebe, P. O. Schmidt, C. Becher, O. Gühne, W. Dür, and R. Blatt, *Nature (London)* **438**, 643 (2005).
- [10] A. B. Klimov, C. Muñoz, A. Fernández, and C. Saavedra, *Phys. Rev. A* **77**, 060303 (2008).
- [11] M. S. Kaznady and D. F. V. James, *Phys. Rev. A* **79**, 022109 (2009).
- [12] D. M. Goyeneche and A. C. de la Torre, *Phys. Rev. A* **77**, 042116 (2008).
- [13] D. Goyeneche, G. Cañas, S. Etcheverry, E. S. Gómez, G. B. Xavier, G. Lima, and A. Delgado, *Phys. Rev. Lett.* **115**, 090401 (2015).
- [14] Q. P. Stefano, L. Rebón, S. Ledesma, and C. Iemmi, *Phys. Rev. A* **96**, 062328 (2017).
- [15] C. Carmeli, T. Heinosaari, M. Kech, J. Schultz, and A. Toigo, *Europhys. Lett.* **115**, 30001 (2016).
- [16] W. Hoppe, *Acta Crystallogr. Sect. A* **25**, 495 (1969).
- [17] J. M. Rodenburg, *Adv. Imaging Electron Phys.* **150**, 87 (2008).
- [18] H. M. L. Faulkner and J. M. Rodenburg, *Phys. Rev. Lett.* **93**, 023903 (2004).
- [19] J. M. Rodenburg, A. C. Hurst, and A. G. Cullis, *Ultramicroscopy* **107**, 227 (2007).
- [20] J. M. Rodenburg, A. C. Hurst, A. G. Cullis, B. R. Dobson, F. Pfeiffer, O. Bunk, C. David, K. Jefimovs, and I. Johnson, *Phys. Rev. Lett.* **98**, 034801 (2007).
- [21] P. Thibault, M. Dierolf, A. Menzel, O. Bunk, C. David, and F. Pfeiffer, *Science* **321**, 379 (2008).
- [22] M. Humphry, B. Kraus, A. Hurst, A. Maiden, and J. Rodenburg, *Nat. Comm.* **3**, 730 (2012).
- [23] Y. Jiang, Z. Chen, Y. Han, P. Deb, H. Gao, S. Xie, P. Purohit, M. W. Tate, J. Park, S. M. Gruner, V. Elser, and D. A. Muller, *Nature (London)* **559**, 343 (2018).
- [24] J. M. Rodenburg and H. M. L. Faulkner, *Appl. Phys. Lett.* **85**, 4795 (2004).
- [25] H. M. L. Faulkner and J. M. Rodenburg, *Ultramicroscopy* **103**, 153 (2005).
- [26] Each wave exiting the probed part of the object can be factorized as $probe \times object$ and each measured far-field intensity must match the square modulus of the Fourier transform of $probe \times object$, respectively.
- [27] M. Reck, A. Zeilinger, H. J. Bernstein, and P. Bertani, *Phys. Rev. Lett.* **73**, 58 (1994).
- [28] In general $\sum_{k=0}^{d-1} |\tilde{c}_{k\ell}|^2 \neq 1$, as the counts will come from the filtered part of $|\psi\rangle$. The renormalization would erase information, so that the raw counts must be used instead.
- [29] Here we are counting the overall number of iterations rather than the PIE iterations which is $(\# \text{ iterations})/n$.
- [30] A. Maiden, D. Johnson, and P. Li, *Optica* **4**, 736 (2017).
- [31] R. W. Gerchberg and W. O. Saxton, *Optik* **35**, 237 (1972).
- [32] M. Guizar-Sicairos and J. R. Fienup, *Opt. Express* **16**, 7264 (2008).
- [33] P. Thibault, M. Dierolf, O. Bunk, A. Menzel, and F. Pfeiffer, *Ultramicroscopy* **109**, 338 (2009).
- [34] M. Stockmar, P. Cloetens, I. Zanette, B. Enders, M. Dierolf, F. Pfeiffer, and P. Thibault, *Sci. Rep.* **3**, 1927 (2013).
- [35] P. Thibault and A. Menzel, *Nature (London)* **494**, 68 (2013).
- [36] J. J. M. Varga, L. Rebón, M. A. Solís-Prosser, L. Neves, S. Ledesma, and C. Iemmi, *J. Phys. B* **47**, 225504 (2014).